Electronic Supplementary Material (ESI) for Journal of Materials Chemistry A.

Supporting Information

Dense Binary Fe-Cu Sites Promoting CO_2 Utilization Enable High Reversible Hybrid Na-CO_2 Battery

Changfan Xu [1], Jing Zhan[1,2*], Huanwei Wang[1], Yao Kang[3], Feng Liang[3]

1. School of Metallurgy and Environment, Central South University, Changsha 410083, China;

2. National Engineering Laboratory for High Efficiency Recovery of Refractory Nonferrous Metals Resources, Changsha 410083, China;

3. Faculty of Metallurgical and Energy Engineering, Kunming University of Science and Technology, Kunming 650093, China

* Corresponding Authors

* E-mail: zhanjing@csu.edu.cn (Jing Zhan); liangfeng@kust.edu.cn (Feng Liang)

Figures and Tables

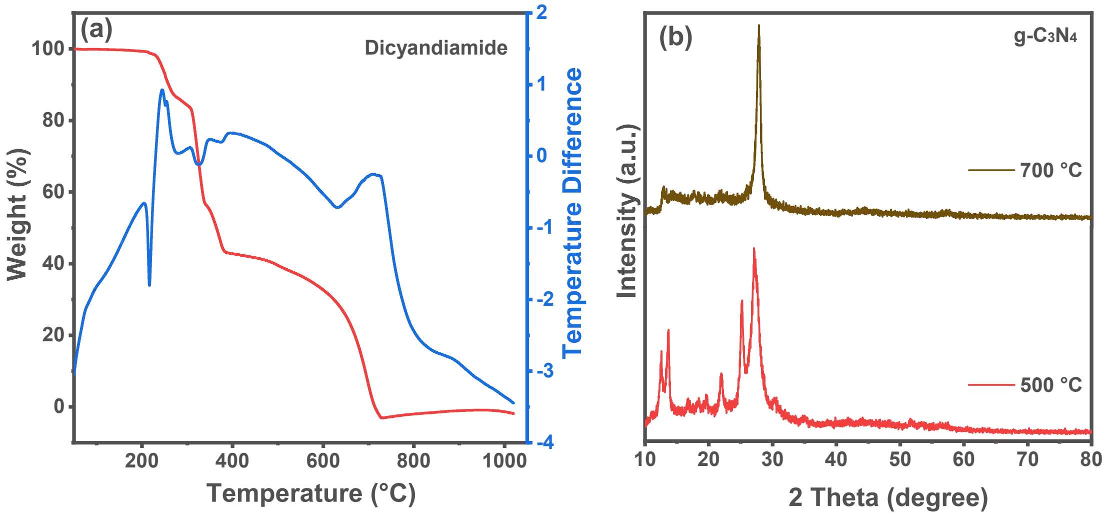

Figure S1 (a) TG-TDA curves of dicyandiamide, (b) XRD patterns of dicyandiamide pyrolysis products at 500 °C and 700 °C in argon

The thermal decomposition behavior of dicyandiamide in argon was first investigated by differential thermal analysis (TG-DSC). As can be seen from Figure S1 (a), the remaining product was zero at temperatures above 720 °C in the argon atmosphere, indicating that the dicyandiamide had completely decomposed and volatilized. As can be seen from the XRD patterns of the dicyandiamide pyrolysis products at 500 °C, 700 °C in Figure S1 (b), the products obtained were all typical of the physical phase of g-C_3N_4 [60]. No carbon material was obtained upon increasing the temperature to 700 °C. It is thus clear that g-C_3N_4 does not generate carbon on pyrolysis in the absence of metal ions.

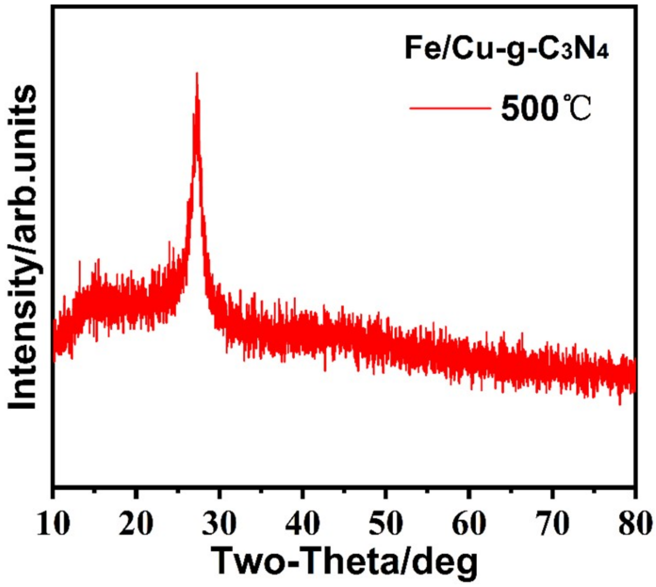

Figure S2 XRD patterns of Fe/Cu-dicyandiamide pyrolysis products at 500 °C in argon

In Fe/Cu-dicyandiamide sample, no peaks corresponding to crystalline metal species such as metal oxides, metal nitrides, metal chlorides, or metal carbides were observed, even when calcined at 500 °C. The absence of metal species peaks suggests that the metal species maintains chemical coordination with the g-C_3N_4 host, most likely in the form of metal–N bonds.

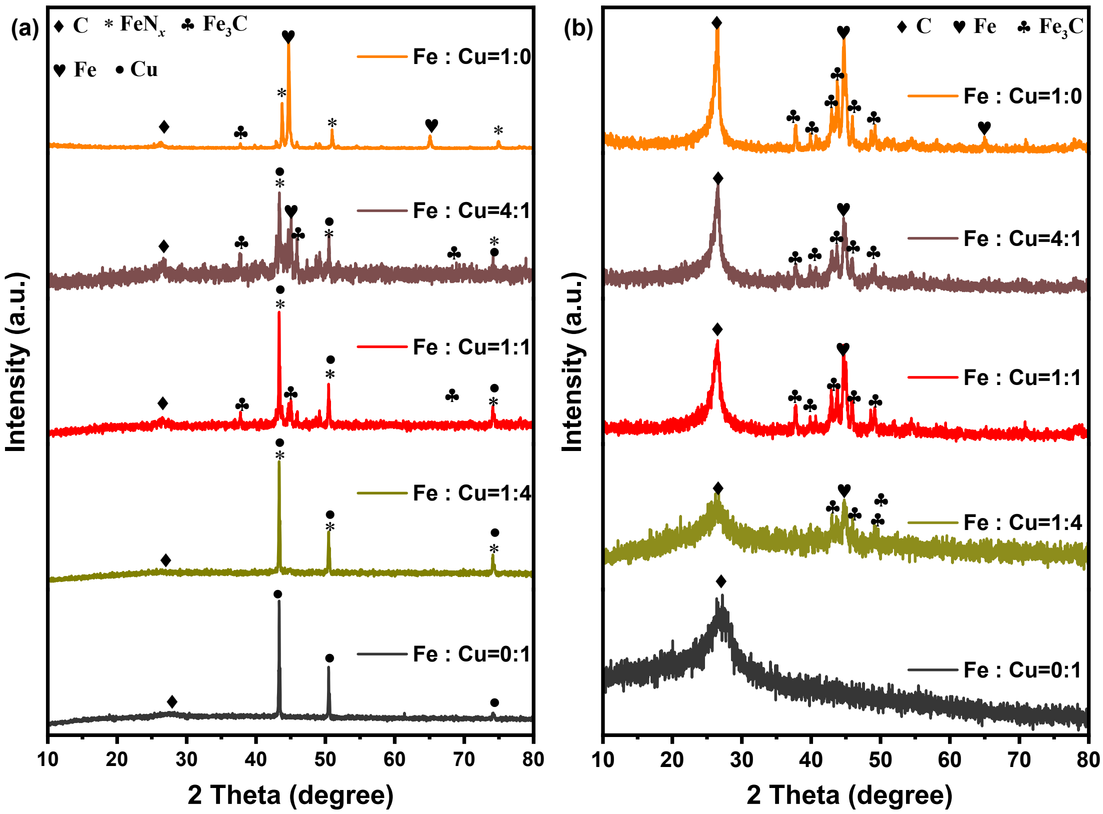

Figure S3 XRD patterns of Fe-Cu-N-C samples obtained with different molar ratios of Fe and Cu (a) before leaching in a solution of H_2SO_4 and $FeCl_3$, (b) after leaching in a solution of H_2SO_4 and $FeCl_3$

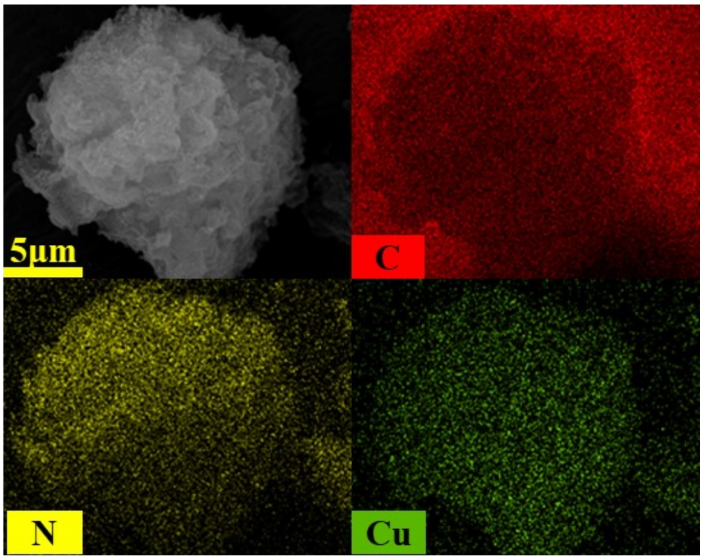

Figure S4 SEM images and the corresponding elemental mapping of Cu-N-C

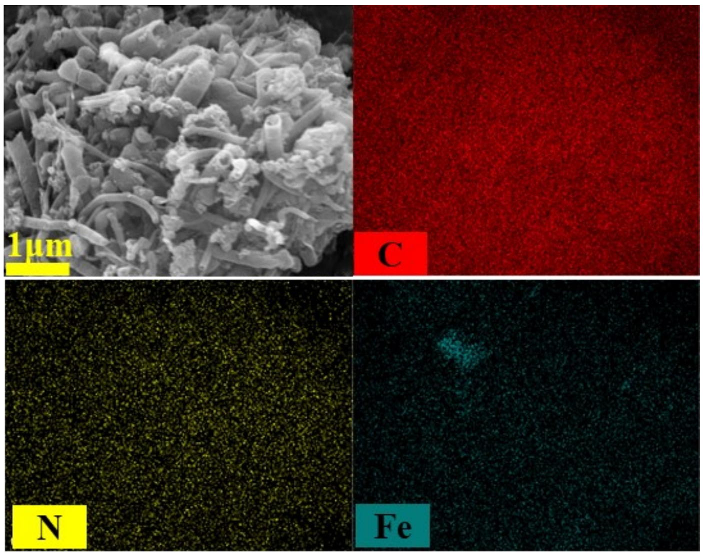

Figure S5 SEM images and the corresponding elemental mapping of Fe-N-C

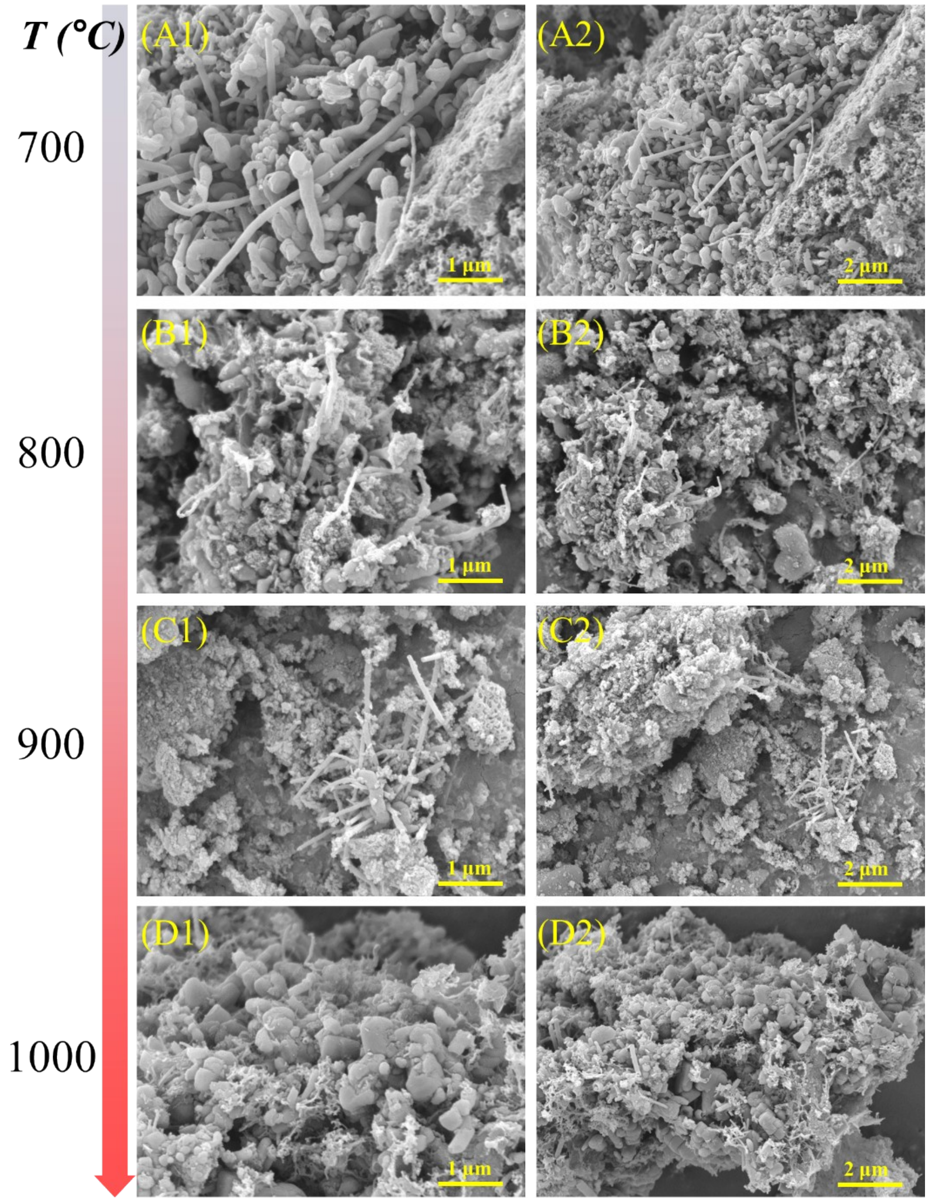

Figure S6 SEM images of Fe-Cu-N-C samples obtained with different heat treatment temperatures (Molar ratio of total metal ions to dicyandiamide: 1:15, and molar ratios of Fe to Cu: 1:1)

(A1–A2) 700 °C, (B1–B2) 800 °C, (C1–C2) 900 °C, (D1–D2) 1000 °C

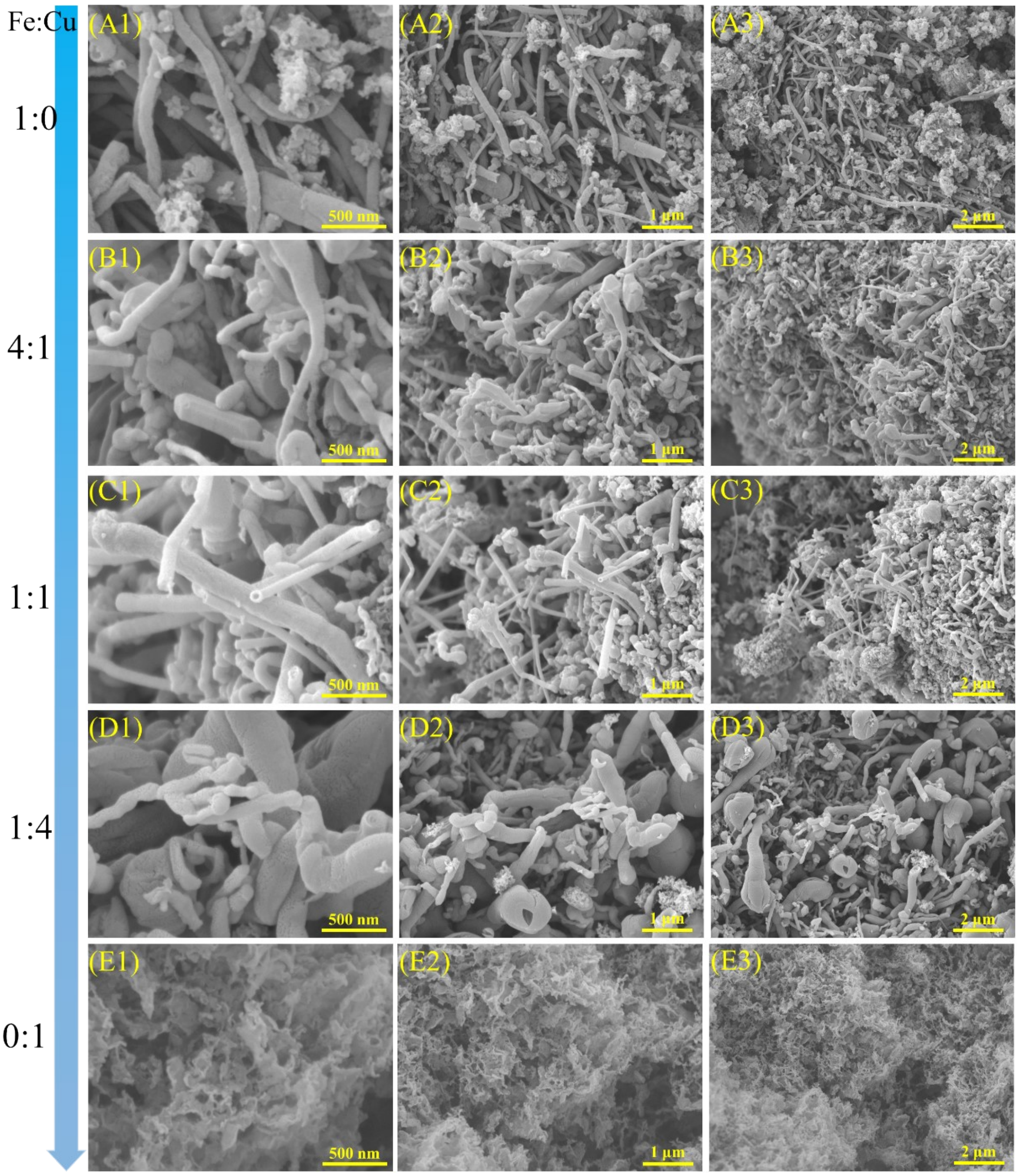

Figure S7 SEM images of Fe-Cu-N-C samples obtained with different molar ratios of Fe and Cu (Molar ratio of total metal ions to dicyandiamide: 1:10, and heat treatment temperature: 700 °C)

(A1–A3) 1:0, (B1–B3) 4:1, (C1–C3) 1:1, (D1–D3) 1:4, (E1–E3) 0:1

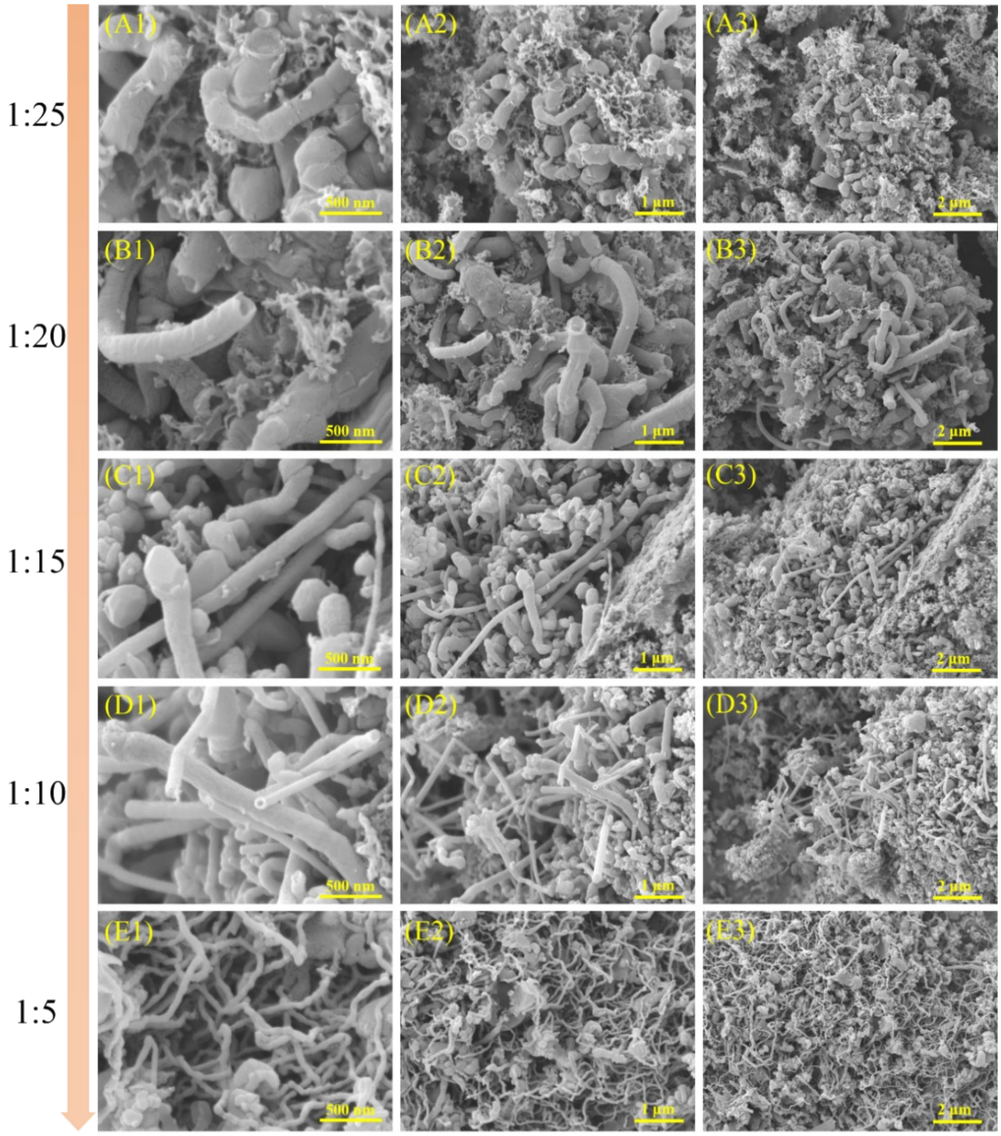

Figure S8 SEM images of Fe-Cu-N-C samples obtained with different molar ratios of total metal ions and dicyandiamide (Molar ratios of Fe to Cu: 1:1, heat treatment temperature: 700 °C)

(A1–A3) 1:25, (B1–B3) 1:20, (C1–C3) 1:15, (D1–D3) 1:10, (E1–E3) 1:5

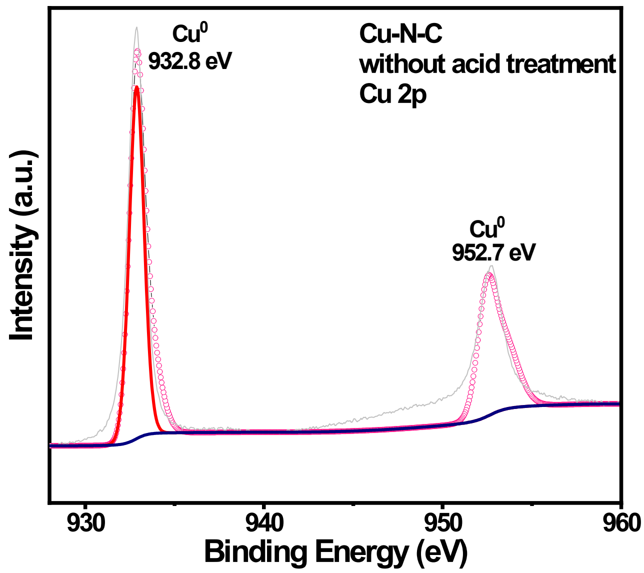

Figure S9 Cu 2p XPS spectra of the Cu-N-C before leaching in a solution of H_2SO_4 and $FeCl_3$

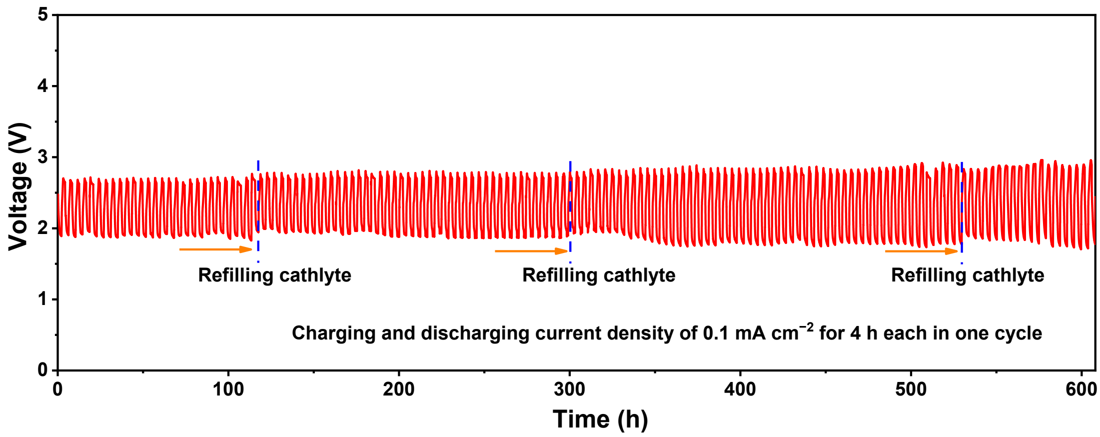

Figure S10 The cycling performance of hybrid Na-CO_2 battery with Fe-Cu-N-C at a current density of 0.1 mA·cm^{-2}, 4 h per cycle

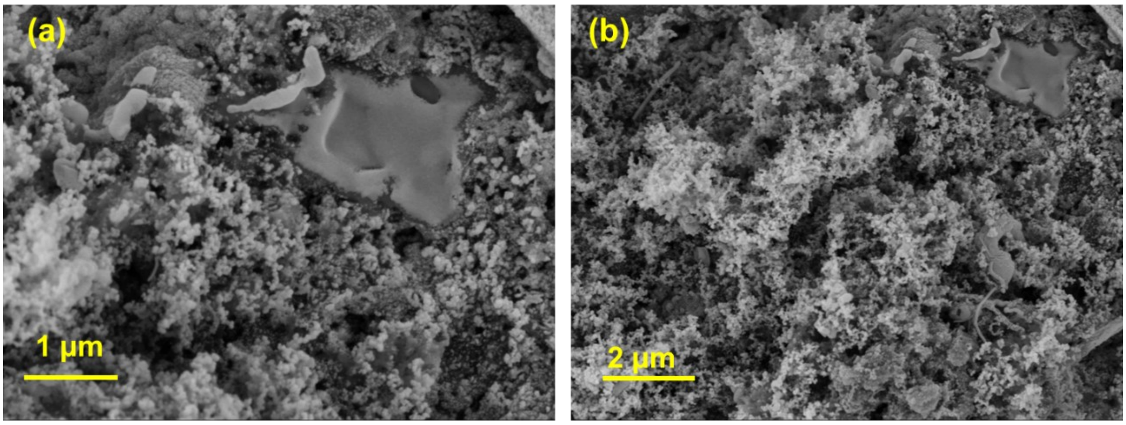

Figure S11 Ex-situ SEM images Fe-Cu-N-C electrode after charge. Hardly any flocculent products were observed.

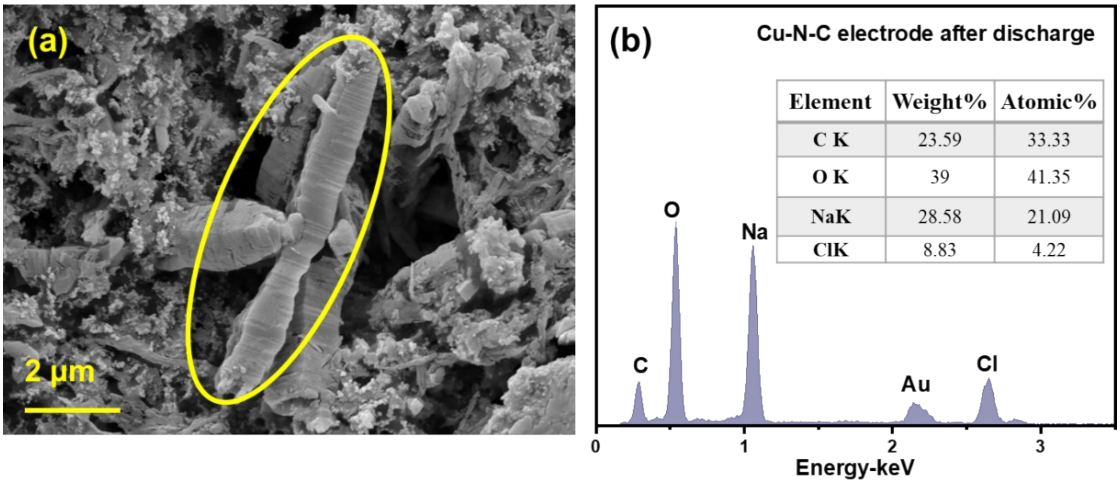

Element	Weight%	Atomic%
C K	23.59	33.33
O K	39	41.35
NaK	28.58	21.09
ClK	8.83	4.22

Figure S12 Ex-situ SEM images and EDS results of Cu-N-C electrode after charge. (The undecomposed discharge products are still present.)

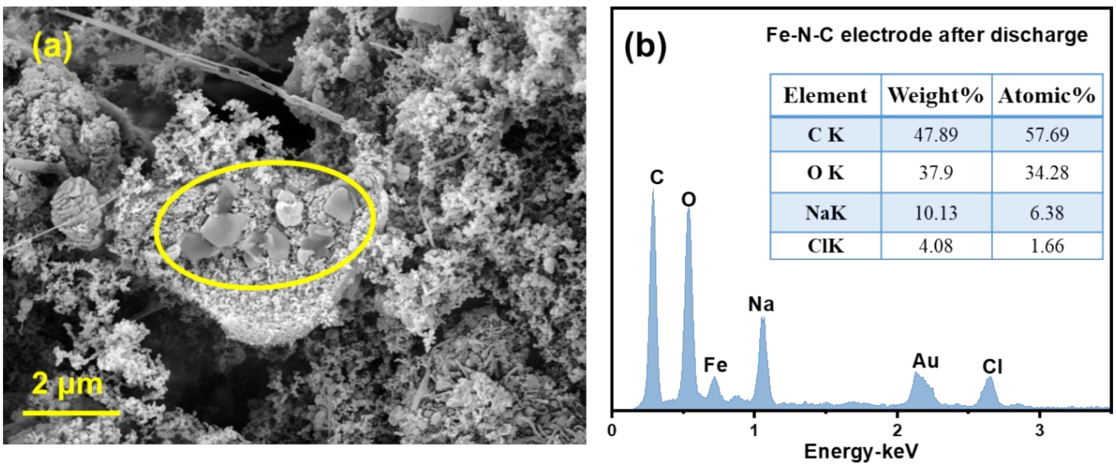

Element	Weight%	Atomic%
C K	47.89	57.69
O K	37.9	34.28
NaK	10.13	6.38
ClK	4.08	1.66

Figure S13 Ex-situ SEM images and EDS results of Fe-N-C electrode after charge. (The undecomposed discharge products are still present.)

Table S1 Specific surface area and pore structure parameters of Fe-N-C, Cu-N-C and Fe-Cu-N-C

Samples	S_{BET} ($m^2 \cdot g^{-1}$)	S_{DFT} a) ($m^2 \cdot g^{-1}$)	V_{DFT} b) ($cm^3 \cdot g^{-1}$)	Average pore Diamete
Fe-N-C	210	175.1	0.716	14.1 nm
Cu-N-C	133	113	0.492	16.0 nm
Fe-Cu-N-C	141	118	0.305	9.06 nm

Table S2 Element atomic percentage of Fe-N-C, Cu-N-C, and Fe-Cu-N-C calculated from XPS results

Sample	Species concentration (at %)				
	C	O	N	Cu	Fe
Fe-N/C	55.49	42.31	2.02	/	0.18
Cu-N/C	59.79	8.4	30.85	0.96	/
Fe-Cu-N/C	50.31	44.14	5.06	0.22	0.28

Table S3 Distribution of each C species, obtained from fitting the C1s XPS spectra results and corresponding characteristic peak position (normalized to the surface C atoms of each material)

Sample	Species concentration (at %)			
	C−C	C−N	C−O/C=O	π−π*
Fe-N/C	39.0 (284.6 eV)	40.9 (285.2 eV)	12.1 (280.0 eV)	8.0 (291.3 eV)
Cu-N/C	41.7 (284.7 eV)	40.6 (286.3 eV)	15.5 (288.1 eV)	2.5 (290.8 eV)
Fe-Cu-N/C	59.2 (284.7 eV)	21.8 (286.1 eV)	13.0 (287.9 eV)	6.0 (291.6 eV)

Table S4 Distribution of each N species, obtained from fitting the N1s XPS spectra results and corresponding characteristic peak position (normalized to the surface N atoms of each material)

Sample	Species concentration (at %)				
	Oxidized−N	Graphitic−N	Pyrrolic−N	M−N_x	Pyridinic−N
Fe-N/C	31.08 (402.75 eV)	25.24 (401.08 eV)	12.69 (399.93 eV)	6.05 (399.06 eV)	24.94 (398.34 eV)
Cu-N/C	3.08 (402.15 eV)	/	35.13 (400.05 eV)	14.41 (399.05 eV)	47.38 (398.38 eV)
Fe-Cu-N/C	12.23 (402.75 eV)	22.59 (401.18 eV)	15.26 (399.98 eV)	20.29 (399.09 eV)	29.64 (398.32 eV)

Table S5 Estimated elemental resistances (R_e, R_i, R_s, R_{ct}, and Z_W) in the equivalent circuits

Sample	R_e (Ω)	R_i (Ω)	R_s (Ω)	R_{ct} (Ω)	Z_W (Ω)
Fe-N-C	64.34	84.98	67.78	19.17	0.975
Cu-N-C	72.16	52.45	67.72	39.9	4.053
Fe-Cu-N-C	72.84	52.07	93.73	6.17	0.133

Table S6 The cyclability of aqueous batteries (including hybrid Li/Na-air/CO_2, Zn-air batteries) between this work and other recently reported results

Cell type	Cathode	Cycling time (h)	Cycling number	Ref.
Hybrid Na-CO_2	**Fe-Cu-N-C**	**610**	**1550**	**This work**
Hybrid Na-CO_2	Co/Co_9S_8@SNHC	160	200	*Materials Today Energy, 2021, 19: 100594*[37]
Hybrid Na-CO_2	N-SWCNH	150	300	*Nano Energy, 2020, 68: 104318.*[49]
Hybrid Na-Air	D-Co-PBA+ Pt/C	340	1000	*Materials Today Energy, 2021, 20: 100572.*[51]
Hybrid Na-Air	Pt_3Ni1/Ni_xFe-LDHs	117	350	*Journal of Materials Chemistry A, 2020, 8(32): 16355-16365.*[52]
Hybrid Na-Air	Fe-NiCoP	170	500	*Applied Catalysis B: Environmental, 2021, 285: 119786.*[53]
Hybrid Na-Air	MOF-NCNTs	100	150	*Dalton Transactions, 2021, 50(20): 7041-7047.*[54]
Hybrid Li-Air	$Nd_{0.5}Sr_{0.5}CoO_{3-d}$	40	20	*Journal of Materials Chemistry A, 2016, 4(6): 2122-2127.*[55]
Hybrid Li-Air	N-MC + NCONF@Ni	420	100	*Energy & Environmental Science, 2014, 7(8): 2630.*[56]
Hybrid Li–Air	Co_3O_4/ON-CNW	540	130	*Nano Energy, 2015, 12: 852-860.*[57]
Zn-Air	CoS_2/SKJ	340	255	*ACS Nano, 2019, 13(6): 7062-7072.*[58]
Zn-Air	FeCo-NCps	156	1400	*Journal of Materials Chemistry A, 2019, 7(20): 12451-12456.*[59]
Zn-Air	NDGs-800	78	234	*ACS Energy Letters, 2018, 3(5): 1183-1191.*[60]
Zn-Air	HHPC	388	1165	*Applied Catalysis B: Environmental, 2020, 265: 118603.*[61]